Hindawi
Journal of Mathematics
Volume 2024, Article ID 9038635, 12 pages
https://doi.org/10.1155/2024/9038635

Research Article

Radiative Mixed Convection Flow of Casson Nanofluid through Exponentially Permeable Stretching Sheet with Internal Heat Generation

Mazhar Hussain, Shereen Fatima, and Mubashir Qayyum

Department of Sciences and Humanities, National University of Computer and Emerging Sciences FAST, Lahore, Pakistan

Correspondence should be addressed to Mubashir Qayyum; mubashir.qayyum@nu.edu.pk

Received 8 November 2023; Revised 14 February 2024; Accepted 15 February 2024; Published 24 February 2024

Academic Editor: Qingkai Zhao

This paper investigates the mixed convection boundary-layer flow of Casson nanofluid with an internal heat source on an exponentially stretched sheet. The Buongiorno model, incorporating thermophoresis and Brownian motion, describes fluid temperature. The modeled system is solved numerically using bvp4c routine to analyze the impact of different fluid parameters on velocity, temperature, and concentration profiles. The analysis reveals that the suction effect, magnetic field, and Casson parameter reduce momentum boundary layer thickness and hence slow fluid motion. Conversely, buoyancy forces increase mass boundary layer thickness which results in accelerating fluid motion. Temperature and concentration profiles show similar trends for Brownian motion, radiation, and thermophoresis.

1. Introduction

In today's era, the exploration of nanofluids has ignited the interest of numerous researchers and scientists due to their remarkable thermophysical attributes, including enhanced thermal conductivity, extensive heat transfer analysis, and superior thermal diffusivity. These attributes have positioned nanofluids as valuable assets with versatile applications across industries, biomedical treatments, consumer appliances, and more. Simultaneously, the analysis of non-Newtonian fluids has garnered substantial importance due to its impact on scientific and engineering applications. These fluids, differing markedly from Newtonian counterparts, are prevalent in daily life and industrial processes, such as toothpaste, mayonnaise, metal extrusion, and more, characterized by non-Newtonian behavior. However, the complexity of these fluids has hindered the establishment of a unified constitutive equation capturing their diverse characteristics. Within this landscape, viscoelastic fluids, such as the Casson model, have emerged as intriguing subjects.

As technological advancements continue to shape our understanding of fluid behavior, it becomes increasingly evident that models like Casson fluid hold immense potential to elucidate complexities related to the non-Newtonian behavior of fluids. In particular, the Casson fluid model can encompass a wide variety of phenomena. Pramanik [1] used this model for analyzing heat transfer characteristics. Raju et al. [2] extended the work of Pramanik by considering radiation and uniform magnetic field. Sources of heat and chemical reactions were explored in his work. The significance of heat transfer can be found in our frequently occurring industrial applications. Few implementations can be found in the process of polymer extrusion, glass blowing, and metallurgical extraction. After Prandtl's boundary layer paper, the idea allowed us to think sensibly and practically for almost any real-world fluid flow situation. Practical implementation was performed by Sakiadis [3], as he was the first one who explored the flow of fluid on a surface that has been stretched. Crane [4] extended his work for both linearly and exponentially stretching sheets in steady two-dimensional flow. Ali [5] presented

general impacts of power law surface with variation of velocity and temperature with the transfer of heat characteristics.

Suction plays an important role in fluid flow as it suppresses the velocity of the flow region. It has several industrial uses and is also commonly utilized in aerodynamics. To provide heat transfer more efficiently, the nanofluid concept has been a blessing due to its thermophysical properties. This innovative technique was introduced by Choi [6] for fluids' thermal conductivity enhancement. Buongiorno [7] suggested a new model based on nanofluid considering the impact of Brownian motion and thermophoresis. Abubakar [8] investigated the nanofluid flow using the Buongiorno model on a stretching sheet. Elbashbeshy et al. [9] extended Abubakar's work to internal heat generation. Dash et al. [10] suggested Casson fluid in a tube with homogenous permeable media. He concluded that when the amount of yielding stress and permeability increases, the flow rate drops dramatically, indicating that frictional resistance increases significantly. Nanjundaswamy et al. [11] presented a flow issue posed across a horizontal sheet and analyzed the impact of mass transfer on the velocity profile. Mahabaleshwar et al. [12] studied ambient nanofluid with suction/injection effects. Recently, Ferdows et al. [13] analyzed dissipative nanofluid on exponentially stretched surface for heat and mass transfer. Recently, Nadeem et al. [14] analyzed 3D Casson fluid through an exponential stretching sheet.

Radiative impacts have many uses in science and engineering. In particular, radiation-based heat transfer has great importance in industrial applications and is hence explored by many researchers. However, the impact of radiation on boundary layer flows is not well explored. Hayat et al. [15] investigated boundary layer flow with thermal radiation using a homotopy-based scheme. Chaudary et al. [16] analyzed heat radiation on viscous fluid flow on a stretched surface in the presence of a uniform magnetic field. Recently, Malik et al. [17] studied heat transfer in the boundary layer of Casson nanofluid flow. Rosly et al. [18] explored unsteady nanofluid with wall mass suction. Numerical results were compared with other researchers' finding. Khan et al. [19] used the Buongiorno model to investigate the nanofluid as Blasius flow. In recent years, many researchers analyzed the above studies focused only on the overstretching sheet. Khan et al. [20] analyzed nanofluid flow over a stretching surface. Makinde et al. [21] studied convective boundary layer nanofluid flow on a stretching sheet. Animasaun et al. [22] investigated Casson fluid on a vertical surface with internal heat generation. Several studies related to different nanofluids with the characteristics of heat and mass can be found in [23–26]. The more interesting studies about stretching sheets related to non-Newtonian fluids flow can be found in [27, 28]. Moreover, Zhu et al. [29] examined the non-Newtonian unstable Williamson fluid on a stretching/shrinking surface, as well as thermophoresis and Brownian effects. Alhamdi et al. [30] focused on numerically solving the problem of micropolar nanofluid using a single-phase model in a channel and also described the behavior of thermal radiation on the temperature profile. It shows that the tube's temperature profile rises from the center to the top wall and falls from the lower wall to the middle.

The following are the primary objectives of this research work:

(1) The present study aims to investigate the convection flow of Casson nanofluid through exponentially stretched sheets with internal heat generation.

(2) The well-known Buongiorno nanofluid model is used to incorporate thermophoresis and Brownian motion.

(3) By using the bvp4c MATLAB package, the obtained reduced ordinary differential equations are solved numerically.

(4) Physical impacts of the Casson parameter, suction effect, magnetic effect, Brownian, and thermophoresis distribution have been presented graphically.

(5) The results that have been described have applicability in thermal extrusion processes, medical treatments, solar energy systems, etc.

2. Problem Formulation

Figure 1 annotates the flow of geometry, i.e., time-independent, incompressible two-dimensional viscous flow of nanofluid.

(1) The sheet is permeable and has been stretched exponentially along a vertical direction at fixed origin, x, and $y = 0$ in xz plane.

(2) Due to the stretching property, the effect on the surface causes the motion of an incompressible non-Newtonian fluid.

(3) Natural convection occurs inside the fluid when temperature changes which produces density variations, resulting in buoyant forces acting directly on the fluid particles.

(4) The flow takes place at the surface parallel to the x-axis.

(5) As depicted in the figure, the magnetic field B_0 is applied perpendicularly in the direction of flow.

(6) Since across the boundary the pressure of the fluid taken into account is constant, it is expected that the induced magnetic field is insignificant in comparison to the applied magnetic field and is thus ignored.

(7) Buongiorno model [1] has been used to study the thermal conductivity of the nanofluid.

$$\tau_{ij} = \begin{cases} 2\left(\mu_B + \dfrac{P_y}{\sqrt{2\pi}}\right)e_{ij}, & \pi > \pi_c, \\ 2\left(\mu_B + \dfrac{P_y}{\sqrt{2\pi}}\right)e_{ij}, & \pi < \pi_c, \end{cases} \tag{1}$$

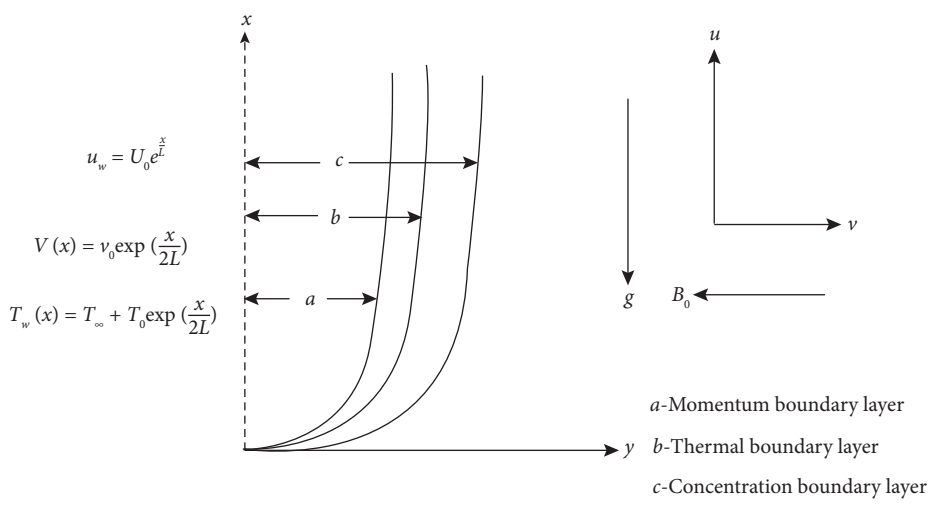

Figure 1: Geometry of flow.

where e_{ij} is the component of the rate of deformation.

$$P_y = \frac{\mu_B \sqrt{2\pi}}{\beta}. \tag{2}$$

The non-Newtonian model's critical value for this product is π_c, and π is the product of the deformation rate component with itself. However, in the Casson fluid, we can assume this $(\pi > \pi_c)$.

$$\mu = \mu_B + \frac{P_y}{2\pi}, \tag{3}$$

incorporating (2) in (3), the following equation of kinematic viscosity is obtained dependent upon the plastic dynamic viscosity of Casson fluid, density, and the Casson parameter β.

$$\nu = \frac{\mu}{\rho} = \frac{\mu_B}{\rho}\left(1 + \frac{1}{\beta}\right). \tag{4}$$

The basic equations governing this fluid flow for the conservation of mass, momentum, thermal energy, and concentration equation for nanofluids according to the Casson fluid model [1] are mathematically written as

$$\begin{aligned}
&\frac{\partial u}{\partial x} + \frac{\partial v}{\partial y} = 0,\\
&u\frac{\partial u}{\partial x} + v\frac{\partial u}{\partial y} = \nu\left(1 + \frac{1}{\beta}\right)\frac{\partial^2 u}{\partial y^2} - \frac{\sigma}{\rho_f}B_0^2 u + g\beta^+ (T - T_\infty),\\
&u\frac{\partial T}{\partial x} + v\frac{\partial T}{\partial y} = \frac{k}{(\rho C_p)_f}\frac{\partial^2 T}{\partial y^2} - \frac{1}{(\rho C_p)_f}\frac{\partial q_r}{\partial y} + \frac{(\rho C_p)_s}{(\rho C_p)_f}\left[D_B \frac{\partial C}{\partial y}\frac{\partial T}{\partial y} + \frac{D_T}{T_\infty}\left(\frac{\partial T}{\partial y}\right)^2\right] - \frac{Q}{(\rho C_p)_f}(T - T_\infty).
\end{aligned} \tag{5}$$

Here, the components of velocity are u and v in x, y directions, ν is kinematic viscosity defined above, β is the Casson parameter, σ is the Stefan–Boltzmann constant, k^* is the absorption coefficient $\alpha = k/(\rho C_p)_f$ is thermal diffusivity in which k is thermal conductivity, C_p is the specific heat, and q_r is the radiative heat flux. $\tau = (\rho C_p)_s/(\rho C_p)_f$ is the relation between the effective heat capacity of the nanoparticle to the fluid's heat capacity, and Q is the coefficient of space-dependent internal heat generation.

By using the approximation of Rossland by Brewster [31], we get the following equation:

$$q_r = -\frac{4\sigma}{3k^*}\frac{\partial T^4}{\partial y}. \tag{6}$$

Considering the Taylor series expansion for T^4 upto T^∞ and exempting higher-order terms $T^4 = 4T_\infty^3 T - 3T^4\infty$, we get the following (7):

$$u\frac{\partial T}{\partial x} + v\frac{\partial T}{\partial y} = \alpha\frac{\partial^2 T}{\partial y^2} + \frac{16\sigma T_\infty^3}{3\rho C_p k^*}\frac{\partial^2 T}{\partial y^2} + \tau\left[D_B\frac{\partial C}{\partial y}\frac{\partial T}{\partial y} + \frac{D_T}{T_\infty}\left(\frac{\partial T}{\partial y}\right)^2\right] - \frac{Q}{(\rho C_p)_f}(T - T_\infty). \tag{7}$$

The concentration equation [32] for the flow model is represented as

$$u\frac{\partial C}{\partial x}+v\frac{\partial C}{\partial y}=D_B\frac{\partial^2 C}{\partial y^2}+\frac{D_T}{T_\infty}\frac{\partial^2 T}{\partial y^2}. \tag{8}$$

The problem's following boundary conditions are provided by

$$\begin{aligned}
&\text{at } y=0,\\
&u=U_w,\\
&v=-V(x),\\
&T=T_w,\\
&D_B\frac{\partial C}{\partial y}+\frac{D_T}{T_\infty}\frac{\partial T}{\partial y}=0,\\
&\text{as } y\longrightarrow\infty,\\
&u\longrightarrow 0,\\
&T\longrightarrow T_\infty,\\
&C\longrightarrow\infty,
\end{aligned} \tag{9}$$

where $V(x)=V_0e^{x/2L}$ is the special type of velocity (Bhattacharyya) [33], $V(x)>0$ is the suction's velocity and is at wall. $U_w=U_0e^{x/L}$ is the stretching velocity, U_0 is the reference velocity (Magyari and Keller [34]), $T_w=T_\infty+T_0e^{x/2L}$ is the temperature at sheet, and T_o is the reference temperature.

3. Solution Method

Incorporating the similarity variables [1] as

$$\begin{aligned}
&\eta=\sqrt{\frac{U_0}{2\nu L}}e^{x/2L}y,\\
&u=U_0e^{x/L}f'(\eta),\\
&v=-\sqrt{\frac{\nu U_0}{2L}}e^{x/2L}\left(f(\eta)+\eta f'(\eta)\right),\\
&T=T_\infty+T_0e^{x/2L}\theta(\eta),\\
&C=C_\infty+C_\infty\phi(\eta).
\end{aligned} \tag{10}$$

Substituting the above similarity variables, the reduced governing equation becomes

$$\begin{aligned}
&\left(1+\frac{1}{\beta}\right)f'''+ff''-2f'^2-2Mf'+2\xi\theta=0,\\
&\left(1+\frac{4}{3}N\right)\theta''+\Pr\left(f\theta'-f'\theta-Q\theta\right)+N_b\phi'\theta'+N_t\theta'^2=0,\\
&N_b\phi''+N_t\theta''+Le(N_b)\left(\phi'f\right)=0.
\end{aligned} \tag{11}$$

Subject to the boundary conditions at

$$\begin{aligned}
\eta&=0,\\
f'&=1,\\
f&=S,\\
\theta&=1,\\
N_b\phi'+N_t\theta'&=0,
\end{aligned} \tag{12}$$

and as

$$\begin{aligned}
\eta&\longrightarrow\infty,\\
f'&\longrightarrow 0,\\
\theta&\longrightarrow 0,\\
\phi&\longrightarrow 0,
\end{aligned} \tag{13}$$

where prime represents the differentiation with respect to η, $\beta=\mu_B\sqrt{2\pi_c}/P_y$ is the Casson parameter, $M=\sigma B_0^2L/\rho_fU_0e^{x/L}$ is the magnetic parameter, $\xi=Gr.1/\mathrm{Re}^2$ is the buoyancy parameter, $N=4\sigma T_\infty^3/kk^*$ is the radiation parameter, $\Pr=\mu C_p/k$ is the Prandtl number, $Q=(Q/(\rho C_p)_f)(2L/U_0e^{x/L})$ is the internal heat parameter, $N_b=\tau D_BC_\infty/\alpha$ is the Brownian coefficient, $N_t=\tau D_T(T_w-T_\infty)/\alpha T_\infty$ is the thermophoresis coefficient, and $\mathrm{Le}=\nu/D_B$ is the Lewis number.

The coefficient of skin friction and Nusselt number can be defined as

$$\begin{aligned}
&\mathrm{Cf}_x=\frac{\tau_w}{\rho_fu_w^2},\quad \text{where, } \tau_w=\mu\left(\frac{\partial u}{\partial y}\right)_{y=0},\\
&\mathrm{Nu}_x=-\frac{Lq_w}{k(T_w-T_\infty)},\quad \text{where, } q_w=-k\left(\frac{\partial T}{\partial y}\right)_{y=0}.
\end{aligned} \tag{14}$$

Applying similarity transformations, the dimensionless form of skin friction and Nusselt number are obtained as

$$\begin{aligned}
2\mathrm{Cf}_x\sqrt{R_{\mathrm{ex}}}&=f''(0),\\
\frac{N_{\mathrm{ux}}}{\sqrt{R_{\mathrm{ex}}}}&=-\theta'(0),
\end{aligned} \tag{15}$$

where $\mathrm{Re}_x=u_wx/\nu$ is the Reynold number.

To obtain the graphical and numerical results using the MATLAB bvp4c package, the reduced governing equation (11) is required to be converted in the first-order ODE.

$$
\begin{aligned}
f &= y_1,\\
f' &= y_2,\\
f'' &= y_3,\\
\theta &= y_4,\\
\theta' &= y_5,\\
\phi &= y_6,\\
\phi' &= y_7,\\
y_1' &= y_2,\\
y_2' &= y_3,\\
y_3' &= \left[-y_1 y_3 + 2y_2^2 + 2My_2 - 2\xi y_4\right]\left(\frac{\beta}{\beta+1}\right),\\
y_4' &= y_5,\\
y_5' &= \left(\frac{3}{3+4N}\right)\left[\left(\Pr y_2 y_4 - y_1 y_5 + Qy_4\right)\right.\\
&\quad \left. - N_b y_5 y_7 - N_t y_5^2\right],\\
y_6' &= y_7,\\
y_7' &= \left(\frac{N_t}{N_b}\right) y_5' - Le y_1 y_7.
\end{aligned}
\tag{16}
$$

Boundary conditions:

$$
\begin{aligned}
y_2 - 1 &= 0,\\
y_1 - S &= 0,\\
y_4 - 1 &= 0,\\
N_b y_7 + N_t y_5 &= 0, \quad \eta = 0,\\
y_2 &= 0,\\
y_4 &= 0,\\
y_6 &= 0,\\
\eta &\longrightarrow \infty.
\end{aligned}
\tag{17}
$$

4. Results and Discussion

Numerical computations have been carried out to analyze the effects of different emerging parameters. M is the magnetic parameter, S is the suction parameter, ξ is the buoyancy parameter, N is the radiation parameter, N_t is the thermophoresis parameter, and N_b is the Brownian parameter over velocity, temperature, and concentration profiles.

To verify the accuracy of the applied numerical scheme, the results corresponding to the values of the heat transfer coefficient $-\theta'(0)$ for Newtonian fluid with $S = Q = M = \xi = Nb = Nt = \mathrm{Le} = 0$ and $N = 0, N = 0.5, N = 1$ are compared with the available published results of Bidin and Nazar [35] with $E = 0$ (the absence of Eckert number) and Pramanik [1] with $S = 0$ (the absence of suction at the boundary).

Figure 2 demonstrates the effect of magnetic Table 1 parameter over the suction velocity. The figure shows a decrement in the suction velocity with the increment of the magnetic parameter. A lower magnetic parameter suggests weaker Lorentz forces, which may result in less dramatic changes in fluid motion caused by the magnetic field. This lower magnetic effect on velocity in the presence of suction shows that the influence of suction dominates over magnetic forces, perhaps allowing for more effective control of fluid motion.

Figure 3 illustrates the effect on the velocity profile concerning the impact of the Casson parameter for the porous sheet. The velocity profile diminishes as the Casson parameter β rises. The declining character of the velocity profile, in particular, suggests a decline in the momentum boundary layer. In other words, when the Casson parameter grows, the region of the fluid immediately impacted by the motion of the porous sheet decreases.

Figure 4 depicts the impacts of suction on the velocity profile for the porous sheet. When suction is increased, the velocity decreases and so does the boundary layer thickness of momentum. The physical elaboration for such kind of behavior can be suggested in easy words as when stronger suction is induced, the heated fluid moves closer to the wall where the effects of viscosity are maximum which decelerates the fluid.

Figure 5 presents the variation of the buoyancy effect on the velocity profile overstretching the porous sheet. The velocity profile grows in proportion to the buoyancy parameter, indicating a higher effect of buoyant forces. This suggests that the fluid velocity near the stretched porous sheet increases as buoyancy effects increase. Furthermore, the observed increase in momentum boundary layer thickness denotes a larger region impacted by the motion of the sheet and the accompanying buoyancy forces.

Figure 6 shows the effects of the magnetic parameter where $(M = 0.1, 0.2, 0.3, 0.4)$ were the values taken to see the effect on the velocity profile for an exponentially porous stretched sheet. The velocity of fluid flow decreases as the magnetic field increases because the magnetic field produces Lorentz force, which opposes the motion of the fluid and hence decreases the motion of the fluid, so the velocity will decrease as the magnetic field increases.

Figure 7 explains the effect on the temperature profile by using the buoyancy parameter. As the buoyancy effect is increased, there has been an impact of decrement in temperature of fluid flow. As buoyant forces depend upon the variation in densities, buoyant forces have an inverse relation with temperature. It can be explained as when we increased the effect of the buoyant force with values

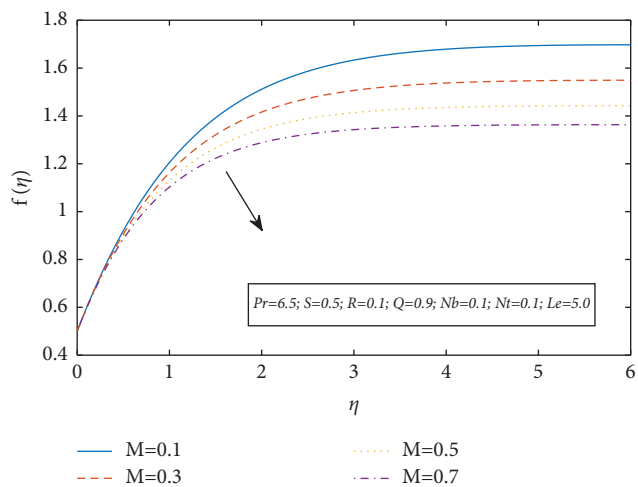

Figure 2: Effects of the magnetic parameter M on suction velocity.

Table 1: Comparison of $-\theta'(0)$ for different values of the Prandtl number.

Pr	Bidin and Nazar [35] with $E=0$			Pramanik [1] with $S=0$			Present study with $S=Q=0$ $M=\xi=\mathrm{Nb}=\mathrm{Nt}=\mathrm{Le}=0$		
	$N=0$	$N=0.5$	$N=1$	$N=0$	$N=0.5$	$N=1$	$N=0$	$N=0.5$	$N=1$
1	0.9547	0.6765	0.5315	0.9547	0.6765	0.5315	0.9432	0.6725	0.5405
2	1.4714	1.0735	0.8627	1.4714	1.0734	0.8626	1.4642	1.0622	0.8520
3	1.8691	1.3807	1.1214	1.8691	1.3807	1.1213	1.8654	1.3725	1.1105

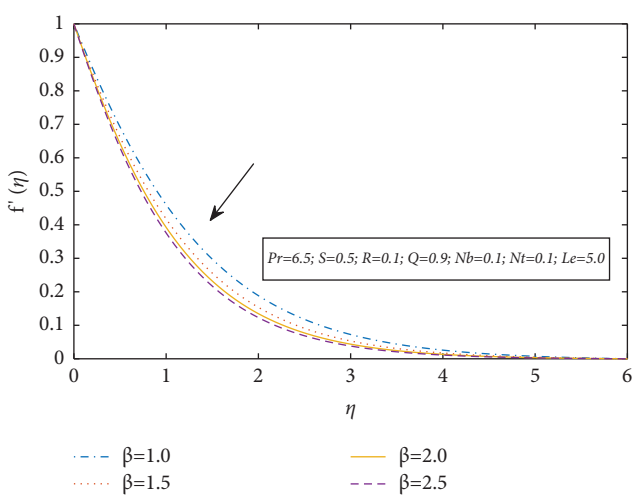

Figure 3: Effects of β (Casson parameter) on velocity.

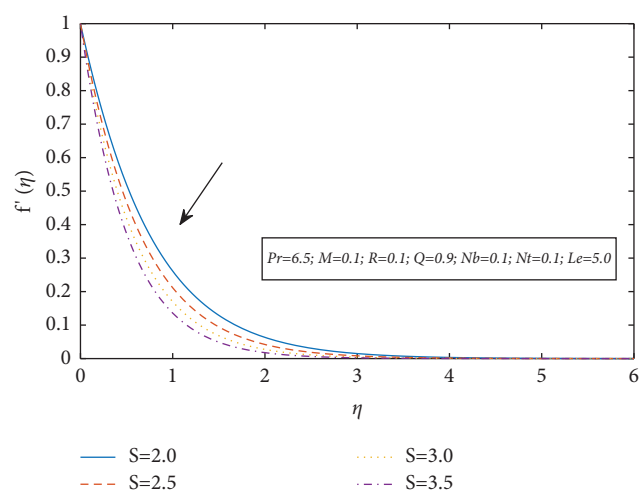

Figure 4: Effects of suction on velocity profile.

($\xi = 0.1, 10.1, 20.1, 30.1$), the density of the fluid increases due to which the temperature decreased.

It has been seen in Figure 8 the effects of the radiation parameter ($N = 0.5, 1.0, 1.5, 2.0$) against the temperature profile. When thermal radiation passes into the fluid, it functions as a source of heat, causing the temperature to rise noticeably. The increased energy causes the fluid molecules to flow faster, causing the temperature to rise. The increased fluid mobility adds to an increase in the thickness of the boundary layer.

Figure 9 elucidates the effect of the Brownian motion parameter ($N_b = 0.1, 0.3, 0.5, 0.7$) on the temperature profile for an exponentially porous stretching surface. The figure explains how with the increment of the Brownian motion parameter, the temperature increases. It is because the temperature is directly proportional to the kinetic energy of the particles and Brownian motion is the movement of fluid particles that causes the fluid particles' kinetic energy to increase, causing the fluid particles to travel faster.

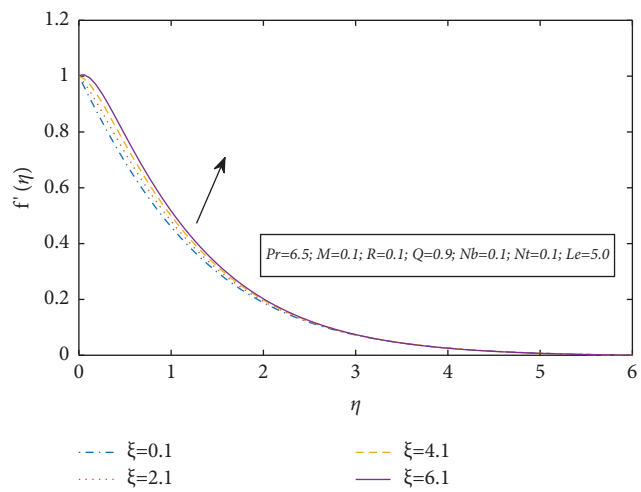

Figure 5: Effects of ξ (buoyancy parameter) on velocity profile.

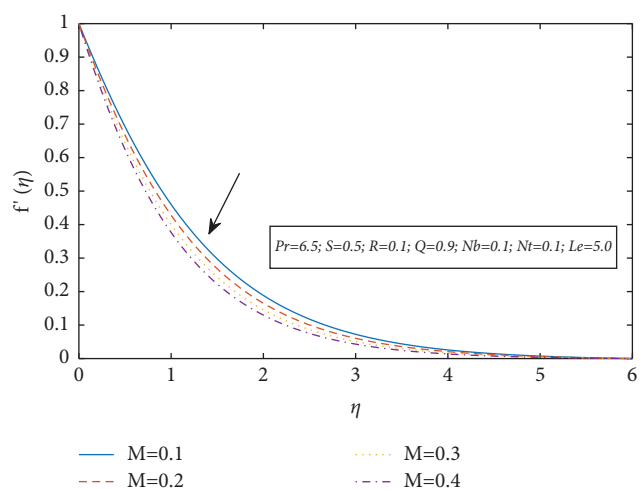

Figure 6: M (magnetic parameter) effects on velocity profile.

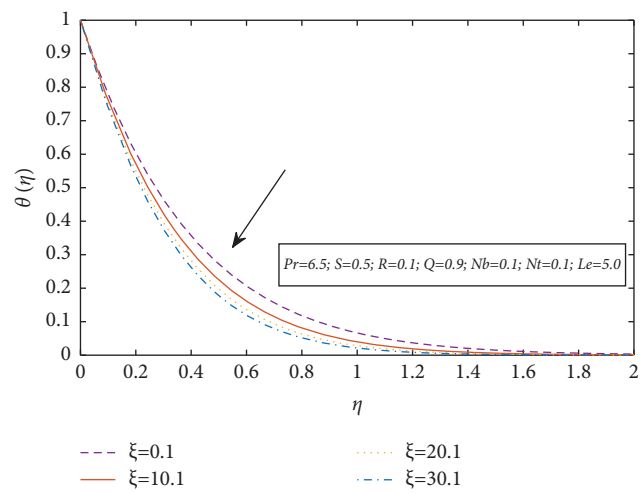

Figure 7: Effects of ξ (buoyancy) on temperature.

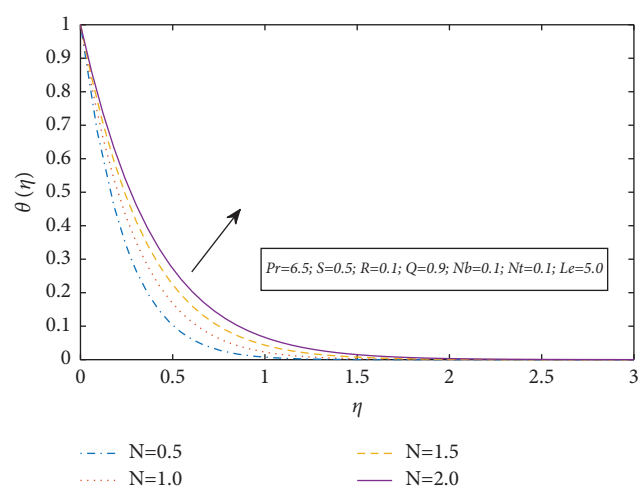

Figure 8: N (radiation) impacts on temperature.

The physical relevance of thermophoresis on fluid temperature resides in its capacity to change temperature distribution throughout the fluid, especially in the presence of microparticles. Figure 10 depicts that the temperature of the fluid rises as the thermophoresis coefficient increases. This effect is caused by thermophoresis, a process in which microparticles move from hotter to cooler locations. As these particles travel, they contribute to improved heat transmission and fluid mixing, resulting in a rise in total temperature.

In Figure 11, a decreasing trend on the fluid concentration profile with the buoyancy effect is seen when $(\xi = 0.1, 10.1, 20.1, 30.1)$. It means that when the buoyancy effect is increased, the concentration of the nanoparticles decreases which decreases the concentration boundary layer thickness.

Figure 12 illustrates the effect of Lewis number on fluid concentration when $(\mathrm{Le} = 1.0, 2.0, 10, 15)$. The thickness of the concentration boundary layer reduces when the value of the Le number is increased as depicted in the figure number is the relation between thermal and mass diffusivity which depicts the fluid flow in which the effect of mass and heat is defined simultaneously.

Figure 13 depicts the effect of thermophoresis on the concentration of nanoparticles when $(N_t = 0.1, 0.3, 0.5, 0.7)$. Thermophoresis causes nonuniformity in concentration distributions of nanoparticles which increases the concentration thickness. The greater the impact of thermophoresis, the greater the effect of the concentration of particles.

Figure 14 depicts the impacts of Brownian motion on nanoparticle concentration. Decrement can be seen that the concentration of nanoparticles is thin when the Brownian parameter's value $(N_b = 0.1, 03, 0.5, 0.7)$ is increased. A shoot of concentration of nanoparticles can be seen before the decrement.

Figure 15 depicts a representation of the concentration of nanoparticles for various magnetic values. As the magnetic parameter's influence grows, so does the concentration of nanoparticles. As the magnetic parameter rises, the magnetophoretic forces impacting the nanoparticles get stronger. These forces efficiently govern the movement and dispersion of nanoparticles in the fluid. As a result, when the magnetic parameter becomes higher, the concentration of nanoparticles increases.

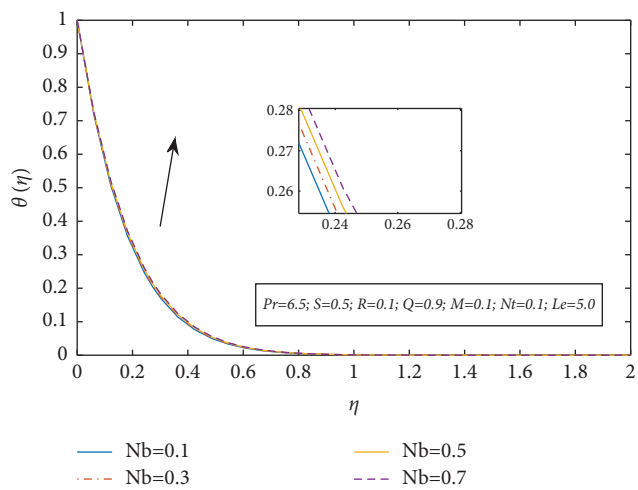

Figure 9: N_b (Brownian motion) impacts on temperature.

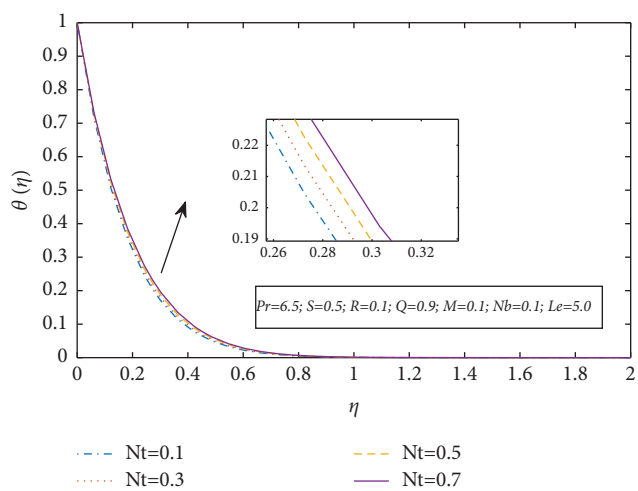

Figure 10: N_t (thermophoresis) impacts on temperature.

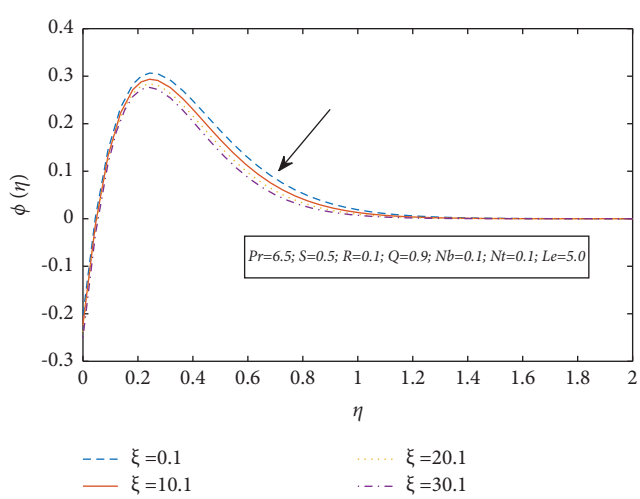

Figure 11: Effects of ξ (buoyancy) on concentration.

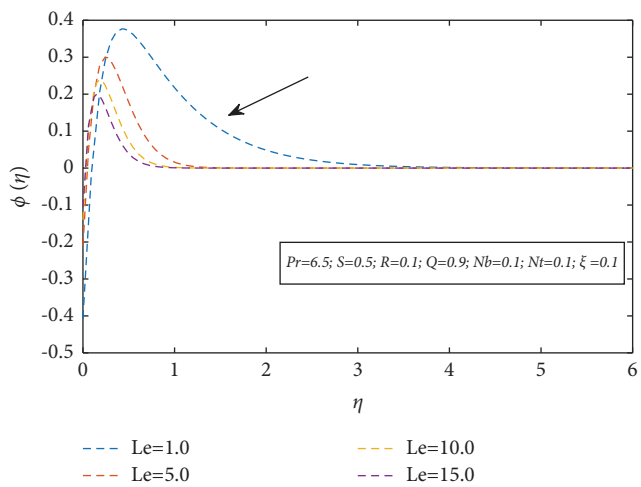

Figure 12: Effects of Le (Lewis number) on concentration.

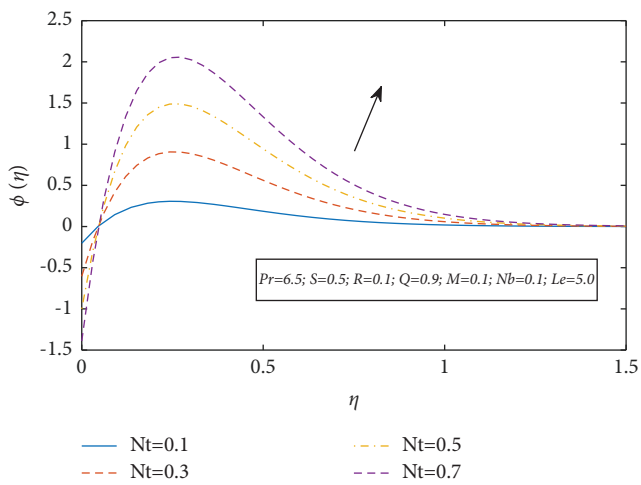

Figure 13: N_t (thermophoresis) effects on concentration.

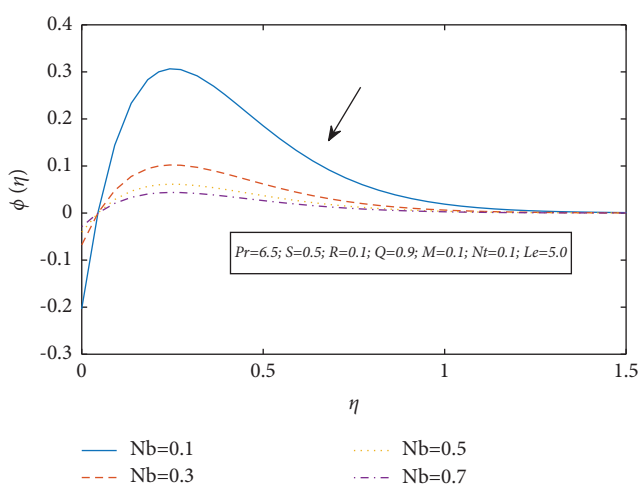

Figure 14: Impacts of N_b (Brownian motion) on concentration.

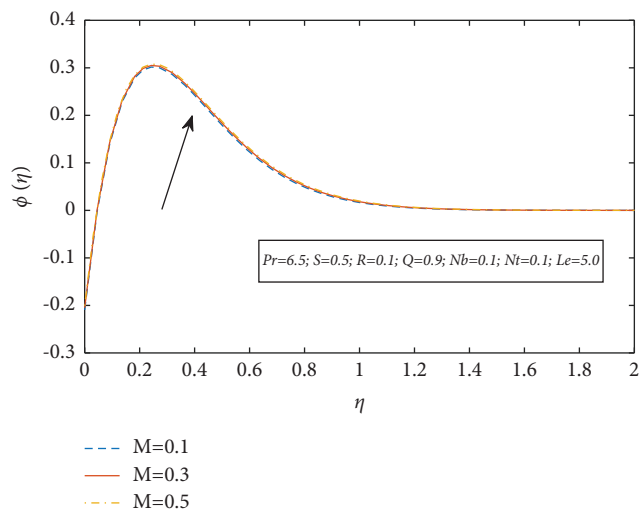

Figure 15: M magnetic effects on the concentration profile.

Table 2: Impact of governing parameters on physical interest quantities.

M	S	N	Q	C_f	N_u
0.1	0.5	2.0	0.9	−0.66189	2.5005
0.3				−0.81007	2.4817
0.5				−0.93561	2.466
0.7				−1.0459	2.4526
0.9				−1.1453	2.4407
0.4	2	2.0	0.9	−1.4139	4.4416
	2.5			−1.6166	5.1916
	3			−1.8273	5.9689
	3.5			−2.0446	6.7665
	4			−2.2672	7.5792
0.4	0.5	0.5	0.9	−0.88597	4.1397
		1		−0.8818	3.312
		1.5		−0.87824	2.8131
		2		−0.87511	2.4735
		2.5		−0.87229	2.2246
0.4	0.5	2.0	−0.2	−0.8686	1.8959
			−0.1	−0.86945	1.9586
			0	−0.87022	2.0184
			0.1	−0.87092	2.0759
			0.2	−0.87158	2.1312

The fluid is subjected to a drag force by the walls, as shown by the negative values of C_f in Table 2, whereas positive values would suggest the reverse effect. Notably, by increasing the radiation, magnetic strength, and suction parameters, the absolute C_f values are rising. The outcome suggests that when N and M values increase, heat transfer rates also increase, while they decrease with suction. Positive Q values suggest a heat source, whereas negative values imply a heat sink effect. The absolute values of C_f and Nu rise with the Q values as they go from the sink to the source.

5. Conclusion

Mixed convection flow of heat and mass transfer analysis of Casson nanofluid through an exponentially stretching sheet was thoroughly investigated. In this work, the Buongiorno model is utilized to enhance the heat transfer, i.e., related to the Brownian movement and thermophoretic distribution of nanoparticles. The impacts of the Casson parameter, suction effect, magnetic effect, Brownian, and thermophoresis diffusion were discussed. In this investigation, the effectiveness of the Casson parameter, suction parameter, magnetic strength, buoyancy impact, thermophoresis parameter, and the Brownian motion parameter on Casson nanofluid through an exponentially stretched sheet was discussed. The result of this numerical analysis led to the following conclusions:

(1) The comparative heat rate transfer is far better than the earlier investigation, which gave rise to trust in the future reporting of the current results.

(2) Casson parameter can be treated as a controlling parameter because velocity suppresses when the Casson parameter values increase and the boundary layer thickness of momentum decreases.

(3) The suction velocity of nanoparticles can be slowed down when the magnetic effect is increased, but it decreases the concentration of nanoparticles.

(4) With the help of the radiation effect, the temperature of the nanoparticles can be escalated.

(5) The buoyancy effect increases the velocity of nanoparticles and decreases the temperature, and due to the density variations, the concentration of nanoparticles decreases significantly, and it depicts the nature of the Grashof number that is proportional to buoyancy forces.

(6) Impact of the Lewis number on the concentration of nanoparticles depicts that increment in the Lewis number decreases the concentration.

(7) Brownian motion increases the temperature, i.e., due to the fast movement of particles, but the concentration of nanoparticles decreases.

(8) Increment of the thermophoresis effect shows the great impact in the temperature and concentration of nanoparticles.

Data Availability

No data were used to support the findings of this study.

Conflicts of Interest

The authors declare that they have no conflicts of interest regarding the publication of this article.

References

[1] S. Pramanik, "Casson fluid flow and heat transfer past an exponentially porous stretching surface in presence of thermal radiation," *Ain Shams Engineering Journal*, vol. 5, no. 1, pp. 205–212, 2014.

[2] C. S. K. Raju, N. Sandeep, V. Sugunamma, M. Jayachandra Babu, and J. V. Ramana Reddy, "Heat and mass transfer in magnetohydrodynamic Casson fluid over an exponentially permeable stretching surface," *Engineering Science and*

Technology, an International Journal, vol. 19, no. 1, pp. 45–52, 2016.

[3] B. C. Sakiadis, "Boundary-layer behavior on continuous solid surfaces: II. The boundary layer on a continuous flat surface," *AICHE Journal*, vol. 7, no. 2, pp. 221–225, 1961.

[4] L. J. Crane, "Flow past a stretching plate," *Zeitschrift für angewandte Mathematik und Physik ZAMP*, vol. 21, no. 4, pp. 645–647, 1970.

[5] M. E. Ali, "Heat transfer characteristics of a continuous stretching surface," *Wärme-und Stoffübertragung*, vol. 29, no. 4, pp. 227–234, 1994.

[6] S. U. S. Choi and J. A. Eastman, "Enhancing thermal conductivity of fluids with nanoparticles," Argonne National Lab(ANL), Argonne, IL USA, ANL/MSD/CP-84938; CONF-951135-29, 1995.

[7] J. Buongiorno, "Convective transport in nanofluids," *Journal of Heat Transfer*, vol. 128, no. 3, pp. 240–250, 2006.

[8] N. A. Abu Bakar, N. Bachok, and N. M. Arifin, "Boundary layer flow and heat transfer in nanofluid over a stretching sheet using Buongiorno model and thermophysical properties of nanoliquids," *Indian Journal of Science and Technology*, vol. 9, no. 31, 2016.

[9] E. Elbashbeshy and M. A. A. Bazid, "Heat transfer in a porous medium over a stretching surface with internal heat generation and suction or injection," *Applied Mathematics and Computation*, vol. 158, no. 3, pp. 799–807, 2004.

[10] R. K. Dash, K. N. Mehta, and G. Jayaraman, "Casson fluid flow in a pipe filled with a homogeneous porous medium," *International Journal of Engineering Science*, vol. 34, no. 10, pp. 1145–1156, 1996.

[11] V. K. P. Nanjundaswamy, U. S. Mahabaleshwar, P. Mallikarjun, M. M. Nezhad, and G. Lorenzini, "Casson liquid flow due to porous stretching sheet with suction/injection," *Defect and Diffusion Forum*, vol. 388, pp. 420–432, 2018.

[12] U. S. Mahabaleshwar, P. N. Vinay Kumar, and M. Sheremet, "Magnetohydrodynamics flow of a nanofluid driven by a stretching/shrinking sheet with suction," *Springer Plus*, vol. 5, no. 1, p. 1901, 2016.

[13] M. Ferdows, K. Zaimi, A. M. Rashad, and H. A. Nabwey, "MHD bioconvection flow and heat transfer of nanofluid through an exponentially stretchable sheet," *Symmetry*, vol. 12, no. 5, p. 692, 2020.

[14] S. Nadeem, R. U. Haq, N. S. Akbar, and Z. H. Khan, "MHD three-dimensional Casson fluid flow past a porous linearly stretching sheet," *Alexandria Engineering Journal*, vol. 52, no. 4, pp. 577–582, 2013.

[15] M. Sajid and T. Hayat, "Influence of thermal radiation on the boundary layer flow due to an exponentially stretching sheet," *International Communications in Heat and Mass Transfer*, vol. 35, no. 3, pp. 347–356, 2008.

[16] S. Chaudhary, S. Singh, and S. Chaudhary, "Thermal radiation effects on MHD boundary layer flow over an exponentially stretching surface," *Applied Mathematics*, vol. 06, no. 02, pp. 295–303, 2015.

[17] M. Y. Malik, M. Naseer, S. Nadeem, and A. Rehman, "The boundary layer flow of Casson nanofluid over a vertical exponentially stretching cylinder," *Applied Nanoscience*, vol. 4, no. 7, pp. 869–873, 2014.

[18] N. S. Rosly, S. Ahmad, and I. Pop, "Unsteady stagnation-point flow past a stretching sheet with suction in a nanofluid using Buongiorno's model," in *Proceedings of The 21st National Symposium On Mathematical Sciences (Sksm21): Germination Of Mathematical Sciences Education And Research Towards Global Sustainability*, pp. 143–148, AIP Conference Proceedings AIP Publishing LLC, Penang, Malaysia, November, 2014.

[19] W. A. Khan, A. Aziz, and N. Uddin, "Buongiorno model for nanofluid blasius flow with surface heat and mass fluxes," *Journal of Thermophysics and Heat Transfer*, vol. 27, no. 1, pp. 134–141, 2013.

[20] W. A. Khan and I. Pop, "Boundary-layer flow of a nanofluid past a stretching sheet," *International Journal of Heat and Mass Transfer*, vol. 53, no. 11-12, pp. 2477–2483, 2010.

[21] O. D. Makinde and A. Aziz, "Boundary layer flow of a nanofluid past a stretching sheet with a convective boundary condition," *International Journal of Thermal Sciences*, vol. 50, no. 7, pp. 1326–1332, 2011.

[22] I. L. Animasaun, E. A. Adebile, and A. I. Fagbade, "Casson fluid flow with variable thermo-physical property along exponentially stretching sheet with suction and exponentially decaying internal heat generation using the homotopy analysis method," *Journal of the Nigerian Mathematical Society*, vol. 35, no. 1, pp. 1–17, 2016.

[23] Y.-X. Li, M. H. Alshbool, Y.-P. Lv, I. Khan, M. Riaz Khan, and A. Issakhov, "Heat and mass transfer in MHD Williamson nanofluid flow over an exponentially porous stretching surface," *Case Studies in Thermal Engineering*, vol. 26, Article ID 100975, 2021.

[24] S. Arulmozhi, K. Sukkiramathi, S. S. Santra, R. Edwan, U. Fernandez-Gamiz, and S. Noeiaghdam, "Heat and mass transfer analysis of radiative and chemical reactive effects on MHD nanofluid over an infinite moving vertical plate," *Results in Engineering*, vol. 14, Article ID 100394, 2022.

[25] W. Abbas and M. M. Magdy, "Heat and mass transfer analysis of nanofluid flow based on Cu, Al2O3, and TiO2over a moving rotating plate and impact of various nanoparticle shapes," *Mathematical Problems in Engineering*, vol. 2020, Article ID 9606382, 12 pages, 2020.

[26] A. Abbasi, W. Farooq, E. S. M. Tag-ElDin et al., "Heat transport exploration for hybrid nanoparticle (Cu, Fe3O4)—based blood flow via tapered complex wavy curved channel with slip features," *Micromachines*, vol. 13, no. 9, p. 1415, 2022.

[27] S. Abdal, I. Siddique, S. Afzal, S. Sharifi, M. Salimi, and A. Ahmadian, "An analysis for variable physical properties involved in the nano-biofilm transportation of sutterby fluid across shrinking/stretching surface," *Nanomaterials*, vol. 12, no. 4, p. 599, 2022.

[28] I. Siddique, M. Nadeem, J. Awrejcewicz, and W. Pawłowski, "Soret and Dufour effects on unsteady MHD second-grade nanofluid flow across an exponentially stretching surface," *Scientific Reports*, vol. 12, no. 1, p. 11811, 2022.

[29] A. Zhu, H. Ali, M. Ishaq, M. S. Junaid, J. Raza, and M. Amjad, "Numerical study of heat and mass transfer for Williamson nanofluid over stretching/shrinking sheet along with brownian and thermophoresis effects," *Energies*, vol. 15, no. 16, p. 5926, 2022.

[30] R. A. Alahmadi, J. Raza, T. Mushtaq, S. A. M. Abdelmohsen, M. R Gorji, and A. M. Hassan, "Optimization of MHD flow of radiative micropolar nanofluid in a channel by RSM: sensitivity analysis," *Mathematics*, vol. 11, no. 4, p. 939, 2023.

[31] M. Q. Brewster, *Thermal Radiative Transfer and Properties*, John Wiley & Sons, Hoboken, NJ, USA, 1992.

[32] D. Ramya, R. S. Raju, J. A. Rao, and A. Chamkha, "Effects of velocity and thermal wall slip on magnetohydrodynamics (MHD) boundary layer viscous flow and heat transfer of a nanofluid over a non-linearly-stretching sheet: a numerical

study," *Propulsion and Power Research*, vol. 7, no. 2, pp. 182–195, 2018.

[33] K. Bhattacharyya, "Boundary layer flow and heat transfer over an exponentially shrinking sheet," *Chinese Physics Letters*, vol. 28, no. 7, Article ID 074701, 2011.

[34] E. Magyari and B. Keller, "Heat and mass transfer in the boundary layers on an exponentially stretching continuous surface," *Journal of Physics D: Applied Physics*, vol. 32, no. 5, pp. 577–585, 1999.

[35] B. Bidin and R. Nazar, "Numerical solution of the boundary layer flow over an exponentially stretching sheet with thermal radiation," *European Journal of Scientific Research*, vol. 33, no. 4, pp. 710–717, 2009.